Magma chamber dynamics in a silicic LIP revealed by quartz: the Mesoproterozoic Gawler Range Volcanics

Agangi, Andrea, McPhie, Jocelyn, Kamenetsky, Vadim S.
ARC-Centre of Excellence in Ore Deposits and School of Earth Sciences, University of Tasmania, Private bag 79, Hobart, Tasmania7001, Australia
Corresponding author: Andrea Agangi, aagangi@utas.edu.au

Abstract

Silicic-dominated large igneous provinces (SLIP) represent vast amounts of magma (≥10^5 km^3) erupted onto the Earth's surface or injected into the crust over short time spans, and are important components of the continental crust. The conditions of formation and evolution of these large magmatic provinces and their magma chambers is still poorly constrained. In this contribution, we examine cathodoluminescence textures and trace element (Al, Ti, Fe) zoning of quartz in a Mesoproterozoic SLIP, the Gawler Range Volcanics (GRV), South Australia. We describe intra-granular textures such as truncation of growth textures and reverse zoning (rimwards increase of Ti content). These characteristics of quartz, together with remelting of already crystallised portions of the magma chamber (felsic enclaves), suggest a complex history of crystallisation and resorption, and fluctuating magma temperature. Titanium-in-quartz geothermometry indicates that adjacent quartz zones record temperature variations (ΔT) up to 70°C in volcanic units. We also report contrasting (non-correlatable) zoning patterns among quartz crystals, each indicating different crystallisation conditions. The juxtaposition of quartz crystals with contrasting zoning patterns are consistent with a dynamic regime (convection, stirring, overturning) of the GRV magma chamber. These results point to pulsating magmatic conditions, compatible with a non-linear evolution of the GRV magma chamber. Heat, necessary to explain both intra-granular and infra-granular textural variations, may have been provided in different pulses by underplating of mafic magma.

Keywords: quartz, crystal stratigraphy, cathodoluminescence, rhyolite, silicic large igneous province, Australia

1. Introduction

Crystal zoning and other disequilibrium textures (mineral rims, resorption textures) are evidence of the occurrence of crystal-melt reactions, and have been used to gain insight into the history of a magma (e.g. Anderson, 1976, 1984; Ginibre et al., 2002). Crystal zoning of different mineral species represents a response to changing conditions, and the succession of growth zones defines a "crystal stratigraphy" (Wiebe, 1968) which yields information on the relative timing of magmatic processes. For example, such textures have been used to infer processes of magma mixing and crustal contamination – considered to occur in the formation and evolution of many intermediate and felsic magmas – even where mixing is complete (hybridisation) or where the magmas involved were similar in composition (e.g. Davidson et al., 2007; Shane et al., 2008;

Streck, 2008; Tepley et al., 2000).

In silicate magmas, quartz is stable under a wide range of compositions and P-T conditions. Despite its abundance, it has not been commonly used as a source of petrological information because quartz has a single end-member composition, and does not readjust its stoichiometric substitutions with changing P-T-X conditions during crystallisation. However, a wealth of information can be recorded in a variety of characteristics of quartz, including habit, non-stoichiometric substitutions in growth zones, inclusions and coronas (e.g. Müller et al., 2003, 2005; Peppard et al., 2001; Sato, 1975; Smith et al., 2010; Wark et al., 2007). The main advantages of quartz in comparison with other minerals are its chemical stability and physical strength. In ancient and altered rocks, quartz may be the only well preserved mineral.

A point of longstanding discussion in the study of silicic-dominated large igneous provinces (SLIP) is the nature of crustal magma storage, including magma chamber geometry and dynamics, and residence time of crystals before eruption. Recent studies have proposed complex models involving zoned magma chambers with variable melt to solid ratio and non-continuous ("waxing and waning") production of melt (Hildreth, 1981; Lipman et al., 1997; Hildreth, 2004; Charlier et al., 2005). Addition of heat and new magma from the mantle can result in "rejuvenation" of the magma chamber (e.g. Hildreth and Wilson, 2007), causing temperature increase, magma mixing, and remelting of crystal mush (largely solid marginal portions of plutons). These variations in magma composition and temperature are potentially recorded by zoned crystals (e.g. Streck, 2008; Vazquez and Reid, 2002).

This study is focussed on the characterisation of quartz populations in the Mesoproterozoic Gawler Range Volcanics of South Australia on the basis of texture, cathodoluminescence, and trace element content. The study involves a wide array of quartz occurrences in different, but genetically associated, volcanic and intrusive rocks (lavas, ignimbrites, shallow and deeper intrusions) to assess the implications of the characteristics of quartz for the magma dynamics in this large igneous province.

2. Geological setting

The Gawler Range Volcanics (GRV) and co-magmatic Hiltaba Suite (HS) granite represent a silicic-dominated large igneous province (the Gawler SLIP) with an outcrop extent of more than 25 000 km^2 and a total estimated volume of 100 000 km^3 (Fig. 1). Although less common than their mafic counterparts, SLIP are being increasingly recognised worldwide. Examples are the Sierra Madre Occidental of Mexico (Bryan and Ernst, 2008; Cameron et al., 1980; Ferrari et al., 2002), the Trans-Pecos volcanic field of the USA (Henry et al., 1988), the Chon-Aike Province of South America and Antarctica (Pankhurst et al., 1998, 2000; Riley et al., 2001) the Snake River Plain of the USA (Branney et al., 2008), and the Whitsunday Volcanic Province of Australia (Bryan, 2007; Bryan et al., 2000). The GRV include several medium- to large-volume (tens to several hundreds of km^3) felsic lavas and ignimbrites (Allen et al., 2008; Blissett et al., 1993) and minor mafic and intermediate units. The Gawler SLIP was emplaced in an intracontinental setting, during the

Laurentian supercontinent assembly (Allen and McPhie, 2002; Allen et al., 2008; Betts and Giles, 2006; Blissett et al., 1993; Creaser, 1995; Giles, 1988) and is coeval with the 1.3 – 1.6 Ga anorogenic magmatic event throughout Laurentia and Baltica (Anderson and Morrison, 2005; Rämö and Haapala, 1995). U-Pb zircon dating of the volcanic units has yielded a narrow age range of 1591-1592 Ma (Creaser, 1995; Creaser and Cooper, 1993; Fanning et al., 1988), whereas ages of the HS granites range from 1583±7 to 1598±2 Ma (Flint, 1993). The Gawler SLIP is associated with a major metallogenic event that affected most of the Gawler Craton (Budd and Fraser, 2004; Fraser et al., 2007; Skirrow et al., 2007; 2002) (Fig. 1).

The GRV have been subdivided into lower and upper sequences (Blissett et al., 1993). The lower GRV consist of thick (up to 3 km) successions, erupted from several discrete volcanic centres. Evenly porphyritic felsic lavas are interbedded with ignimbrites and very minor volcanogenic sedimentary facies. Several units have been intruded by felsic porphyritic dykes. The Chitanilga Volcanic Complex at Kokatha (Blissett, 1975, 1977a, 1977b; Branch, 1978; Stewart, 1994) and Glyde Hill Volcanic Complex at Lake Everard (Blissett, 1975, 1977a, 1977b; Ferris, 2003; Giles, 1977) are the two best exposed parts of the lower GRV and are the subject of this study. The upper GRV are composed of three large-volume (>500 km^3) evenly porphyritic felsic lavas (Allen and McPhie, 2002; Allen et al., 2008; McPhie et al., 2008). The GRV are essentially undeformed and unmetamorphosed and primary textures are well preserved, in spite of the moderate, although widespread alteration of feldspar. The GRV sequence is cross-cut by numerous porphyritic, rhyolite and, less abundant andesite, dykes. These dykes are up to 100 m wide and 10-20 km long, and mostly trend northwest to north-northeast (Blissett et al., 1993). The Moonamby Dyke Suite (Giles, 1977) includes quartz-feldspar-phyric dykes that intruded the lower GRV at Lake Everard. The Hiltaba Suite includes large batholiths and smaller intrusions of granite and minor quartz monzodiorite and quartz monzonite (Flint, 1993). Typical of much of the Hiltaba Suite is medium-grained, locally porphyritic pink granite composed of quartz, alkali-feldspar, minor plagioclase, biotite, apatite and fluorite.

3. Methods and analytical techniques

Whole-rock analysis

Samples were crushed in a WC mill for X-ray fluorescence (XRF) and inductively coupled plasma mass spectrometry (ICP-MS) whole-rock analysis at the University of Tasmania. Major and some trace elements (V, Cr, Ni, Cu, Zn, Rb, Sr, Y, Zr, Nb, Ba, and La) were measured by XRF, trace elements were analysed by ICP-MS. Samples were digested in HF/H_2SO_4 with the PicoTrace high pressure digestion equipment and analysed with an Agilent 4500 ICP-MS. XRF analyses were made on a Philips PW1480 X-ray Fluorescence Spectrometer. Detection limits for trace elements in ICP-MS are ≤0.01 ppm (REE) and ≤0.5 ppm for other elements, except As (5 ppm). Comparison of XRF and ICP-MS trace element data indicates a good correlation between the two methods, the difference being <20 % for all elements analysed by both methods, except Ba.

Scanning electron microscope cathodoluminescence (SEM-CL) imaging

Cathodoluminescence (CL) images were obtained with a FEI Quanta 600 scanning electron microscope (SEM) operated at 10 kV and equipped with a Gatan PanaCLF CL detector. All CL images are polychromatic (including all wavelengths) 8 bit bitmap (grey scale values in the range 0-255). Core-to-rim CL intensity profiles were obtained by measuring the local grey value in an area approximately 20 X 20 µm. CL profiles were obtained in areas free of healed fractures, inclusions and surface irregularities.

Quartz trace element analysis

Trace element concentrations in quartz were determined by a Cameca SX-100, 5 detector-equipped electron microprobe operating at 15 kV and 200 nA, 5 µm beam diameter and 720 s counting time. Analyses were performed for Al, Ti and Fe along core-to-rim traverses. Corundum, hematite and rutile were used as standard minerals. In order to test the repeatability of the measurements, each traverse was repeated in two closely spaced parallel lines. Detection limits, calculated from counting statistics, are: Al 9 ppm, Ti 14 ppm, Fe 23 ppm; standard deviations are: Al 8 ppm, Ti 12 ppm, Fe 19 ppm.

4. Sample description (Table 1)

4.1 Volcanic units

Three evenly quartz-phyric volcanic units (Wheepool Rhyolite, Waurea Pyroclastics and Lake Gairdner Rhyolite) are present in the Glyde Hill and Chitanilga Volcanic Complexes of the lower GRV. Quartz occurs as subhedral (bipyramidal) to anhedral (round and embayed) crystals or as angular fragments, up to 2 mm in size.

The Wheepool Rhyolite (samples GH06, 23, 24c, 59) includes massive or flow-banded porphyritic lavas. Phenocrysts (~10 vol.%) comprise euhedral to subhedral plagioclase (albite) and K-feldspar (perthite), and minor (≤1 vol.%) subhedral to anhedral quartz, mostly ≤1 mm in diameter. The microcrystalline to micropoikilitic groundmass (<10 to 50 µm) is mainly composed of quartz, K-feldspar and albite (Fig. 2a).

The Lake Gairdner Rhyolite (samples GH51, 87) contains massive to eutaxitic, fiamme-bearing ignimbrite with quartz, K-feldspar (perthite) and plagioclase (albite) crystals and crystal fragments (≤2 mm, ~20 vol.%), and minor lithic fragments in a fine grained, eutaxitic-textured matrix. Quartz crystals are sub- to euhedral (bipyramidal). The matrix is mainly composed of platy and cuspate devitrified glass shards, <0.5 mm in size.

The Waurea Pyroclastics (samples GH13, 95) include several different pyroclastic facies that vary in grain size, composition and texture. The observed samples are from one of these facies, composed of violet to pale grey, relatively poorly-sorted crystal tuff. It contains quartz as a major component (5-10 vol.%), other than K-feldspar, minor plagioclase (albite), and lithic fragments (<5 vol.%). Quartz occurs as anhedral (round to lobate) to subhedral crystals and angular crystal fragments, ≤1-2 mm in diameter, and is present as separate crystals or included in lithic fragments. The matrix is fine grained (≤0.3 mm) and mainly composed of devitrified glass shards.

4.2 Dykes

The Glyde Hill Volcanic Complex is intruded by the Moonamby Dyke Suite (samples GH15, 70, 70B, 92). The dykes are up to tens of metres wide, show mostly homogeneous texture and contain medium- to coarse-grained phenocrysts (≤30 mm) of K-feldspar, quartz and minor sodic plagioclase (Fig. 2b). The quartzo-feldspathic groundmass is microcrystalline (grain size ≤50 μm) to poikilitic. Quartz phenocrysts are anhedral and deeply embayed (or “vermicular”).

4.3 Hiltaba Suite granite

The Hiltaba Suite (samples GH37, 38) at Kokatha consists of leucocratic, equigranular to seriate granite, mainly composed of quartz, K-feldspar, plagioclase and biotite. The granite is medium to coarse-grained (≤10 mm, sample GH37), and locally finer grained (≤a few mm, sample GH38). Quartz and K-feldspar show mutual inclusion relationships and intergrowth (granophyric) textures are also present.

4.4 Felsic enclaves

Enclaves of granite (sample GH29, 32) included in some of the volcanic units are centimetres to several metres in size, and unfoliated. They contain mm-scale crystals of K-feldspar and amoeboid quartz, separated by a microcrystalline quartz +K-feldspar +albite groundmass (Fig. 2c). Feldspar phenocrysts are surrounded by a granophyric rim, up to 0.5 mm thick, formed by an intergrowth of K-feldspar and quartz crystals oriented perpendicular to the margins of phenocrysts (Fig. 2d). These intergrowths make up 10-20 vol.% of the groundmass. The enclaves occur in several felsic lava units and have round and gradational margins with the host rock. Around the enclaves, the host rock contains scattered anhedral quartz and K-feldspar crystals.

4.5 Geochemistry

The Gawler SLIP has a wide SiO_2 compositional range (Fig. 3, Table 2; Giles, 1988); with a sharp predominance of felsic rocks (> 90% in outcrop, Allen et al., 2008). The rocks are characterised by high K_2O (up to 7-8 wt.%), are calc-alkalic to alkali-calcic in the modified alkali-lime plot (Frost et al., 2001), and are metaluminous to mildly peraluminous (aluminium saturation index ≤1.1-1.2). Locally higher aluminium saturation index values are interpreted as due to alteration. Rare earth elements, Y, and Zr increase with silica and peak at ~70 wt.% SiO_2. Other high field strength elements (Nb, Ta, and Th) and Rb increase even in the most silica-rich compositions. All samples used in this study plot in the rhyolite field in the total alkalis vs silica diagram (Fig. 3). Primitive mantle-normalised plots (Fig. 3) have similar trends with Ba, Sr, Ti, P, and Eu negative spikes, and slightly decreasing rare earth element distributions (La_N/Yb_N = 12±3.5, n = 12).

5. Intra-granular textures and zoning of quartz

5.1 Quartz cathodoluminescence

CL images can highlight cryptic intra-granular textures, undetectable in both optical and back-scattered electron (BSE) microscopy. These textures include: 1) growth-related textures (growth zones), twinning, grain shapes and growth modes (e.g. D'Lemos et al., 1997); 2) resorption-related textures, indicated by intersection relationships between growth surfaces (“unconformity”); 3) healed brittle deformation structures. Other than being an intrinsic characteristic of each mineral, CL is strongly dependent on defects in the crystal lattice, particularly point defects induced by trace element substitutions, or “activators”. Therefore, CL can be used as a proxy for trace element distribution (e.g. Müller et al., 2000; Perny et al., 1992; Watt et al., 1997).

CL textures are referred to as primary and secondary, in reference to textures formed during and after crystallisation, respectively. Among primary textures, oscillatory and step zones are defined by similarity with compositional zones in plagioclase (Sibley et al., 1976; Watt et al., 1997). Oscillatory zones are periodic, small-scale (µm-scale) and small-amplitude variations in CL and are considered to be due to slow, diffusion-controlled crystallisation under conditions of low oversaturation (Bottinga et al., 1966; Shore and Fowler, 1996; Sibley et al., 1976). These conditions are possible in a relatively static magma which preserves diffusive boundary layers at the crystal-liquid interface (Allègre et al., 1981; Sibley et al., 1976). Thus, oscillatory zones are interpreted to be the result of local self-organisation of trace elements at the interface between melt and crystal. Conversely, step zones are defined as wide, non-periodic and larger-scale (≥tens of µm) variations in CL intensity. Unlike oscillatory zones, step zones are interpreted to be due to “external” or “extrinsic” factors independent of local crystallisation and reflect variations in intensive parameters (P, T) and magma composition caused by processes such as crystal settling, magma convection, mixing, and reservoir replenishment (Shore and Fowler, 1996).

The most common secondary textures are healed fractures, healed radial cracks around melt and fluid inclusions, and modifications (“smudging”) of primary zones due to redistribution of lattice defects (e.g. Boiron et al., 1992; Götze et al., 2005; Müller et al., 2010).

Comparison of CL images allows groups of crystals with similar zoning patterns to be identified; zones can be correlated among crystals in the same group. The classification of CL textures is subjective. The following classification criteria have been adopted: presence of step zones and oscillatory zones, intersection between CL textures, CL intensity and shape of step zone margins. Crystals from each unit show one or more CL zoning patterns.

5.1.1 Volcanic units (samples GH06, 23, 59, 13, 95, 51, 87)

Comparison of approximately 120 grains reveals three main CL step zones (1-3, Fig. 4). Observed crystals consist of one (2, 3) or two zones (1, 3; 2, 3). Zone (1) is CL-dark, homogeneous or progressively darker towards the rim, and locally oscillatory zoned. Zone (1) occurs as anhedral crystal cores rimmed by zone (3). The contact between zones (1) and (3) discordantly truncates internal growth (oscillatory) zones. Zone (2) is CL-bright and oscillatory zoned. Zone (2) has round margins and either occurs as cores discordantly surrounded by zone (3) or forms the whole crystal. Zone (3) is relatively CL-bright, oscillatory zoned, and has euhedral to subhedral concordant margins. Zones (1) and (2) were not found in contact. Crystals apparently formed by zone (3) only (Fig. 4c, g) may be artefacts of sectioning. Oscillatory zones in zones (1), (2), and (3) are mostly planar and parallel, indicating that the crystals maintained euhedral shapes throughout most of their growth. In addition to zones (1) to (3), thin (<100 µm), irregular-bordered bright rims are locally present around phenocrysts (Fig. 4a). These rims have similar CL characteristics to the groundmass quartz.

5.1.2 Dykes (samples GH15, 70, 70B, 92)

Approximately 120 CL images of more than 70 quartz grains from three different dykes of the Moonamby Dyke Suite were compared. Unlike in the volcanic units, the main step zones are similar and can be correlated between crystals in each dyke, although significant differences can be seen among different dykes (Fig. 5). Step zones are evident in two of the dykes and are superimposed by planar (euhedral) to irregular and convoluted oscillatory zones (Fig. 5a-d). Numerous quartz grains have lobate growth surfaces (oscillatory zones). Some lobes extend outwards and define embayments at the grain margin or have been overgrown, resulting in the formation of melt inclusions (Fig. 5c, d).

In dyke 1 (samples GH70, 70B), three main CL step zones, separated by sharp boundaries, can be distinguished (core, mantle, rim; Fig. 5a-c). The core is bright and anhedral and has lobate margins. The core is surrounded by a CL-dark mantle, in which oscillatory zones overall decrease in luminescence towards the rim. Both the core-mantle and the mantle-rim boundaries discordantly truncate the internal textures. In a few cases, the mantle-rim boundary cuts through the mantle and into the core (Fig. 5b). The rim is relatively bright and homogeneous. In addition to these three step zones, phenocrysts are locally overgrown by a bright, thin (<20 µm), and homogeneous external layer of quartz. This layer has similar characteristics to the microcrystalline groundmass quartz.

In dyke 2 (GH15), two or three broadly concentric step zones (Fig. 5d) are separated by transitional contacts. Wavy or lobate growth surfaces (oscillatory zones) are mainly limited to discrete intervals, mostly occurring in the rim and, occasionally, in the core. Minor truncations surfaces, not associated with abrupt CL changes, occur within different step zones.

In dyke 3 (sample GH92), phenocrysts show weakly contrasted oscillatory zones without step zones. The “smudging” of oscillatory zones makes the relationship between habit and growth textures unclear (Fig. 5e).

5.1.3 Hiltaba Suite granite (sample GH37)

Comparison of 15 quartz grains shows a weakly contrasted CL emission with rather irregular distribution. Two zoning patterns were distinguished. The first pattern (Fig. 6a) has two nearly concentric step zones (core and rim). The core is bright and homogeneous; the rim is oscillatory zoned and becomes progressively darker towards the grain margin. The core-rim boundary is gradational. The core does not show internal textures, whereas the rim contains weakly contrasted oscillatory zones. The anhedral grain margins cut across the oscillatory zones in the rim. The second pattern is characterised by a weakly contrasted to homogeneous, non-concentric luminescence. The growth zones are weakly defined and do not allow detailed characterisation (Fig. 6b).

5.1.4 Felsic Enclaves (samples GH29, 32)

In felsic enclaves, quartz crystals are characterised by weakly contrasted zones without step zones. Weakly contrasted oscillatory zones are cross-cut by the grain margin (Fig. 6c). In some crystals, CL textures are “smudged” and no concentric zones were observed. A thin CL-bright overgrowth, showing similar characteristics to the groundmass, discontinuously rims the quartz phenocrysts.

5.1.5 Secondary textures

Healed fractures are clearly distinguishable in CL as low emission (dark grey-black) bands, up to a few tens of µm wide. In the granite and some of the dykes, healed cracks form a dense network throughout quartz crystals. Trails of fluid inclusions are aligned along fracture traces. Weakly luminescent areas, characterised by irregular shape and sharp margins, are present in several samples (Fig. 5e, 6b-c). These areas are not spatially related (discordant) to the primary concentric zones and appear to be at least partially related to fractures and grain boundaries. Apparently similar textures were reported by (D'Lemos et al., 1997; Van den Kerkhof and Hein, 2001).

5.2 Quartz trace element content

Trace element concentrations in different CL zones were determined in core-to-rim microprobe profiles (Fig. 7, Table 3). The different CL zones are characterised by different trace element contents (Fig. 8). The total range in Ti concentration is approximately 20 to 130 ppm and Ti abundance shows a positive correlation with CL intensity (Fig. 7, 8). The correlation between Ti concentration and the blue ~420-nm CL emission has been found in other studies (e.g. Müller et al., 2002) This is a prominent emission that dominates panchromatic images, and justifies the use of CL brightness as a proxy for Ti distribution (e.g. Müller et al., 2005; Wark and Watson, 2006). Iron content is in the range 10-330 ppm; Al is in the range 100-680 ppm and in places it is above 3000 ppm. Aluminium and Fe abundances are not correlated with CL, and no clear correlation was found between trace elements. Abundances of Ti in adjacent analyses along parallel traverses are very similar, the differences being comparable with, or less than, analytical error. Iron abundances are also similar in adjacent analyses. Conversely, Al content locally is significantly different, in the order of several tens to hundreds of ppm. Such differences may be due to the presence of microinclusions or surface contamination introduced during the polishing process with alumina powder.

6. Discussion

6.1 Crystallisation history of quartz recorded by crystal stratigraphy

When interpreting compositional zones of crystals, comparisons are made on core-to-rim profiles and between crystals or crystal populations. When analysing single profiles, stepped profiles, commonly associated with dissolution and indicating compositional breaks, are contrasted with smooth profiles, indicating gradual changes of intensive parameters or composition. When comparing zones of different crystals, the following combinations can be envisaged: 1) crystal cores and rims are similar (correlatable), 2) cores are similar, but rims are different, 3) cores are different, but rims are different, and 4) cores and rims are different (e.g. Wallace and Bergantz, 2005).

Planar and parallel CL growth zones (Fig. 4) indicate that the crystals were euhedral and their facets remained parallel during crystallisation. Wavy and lobate CL growth zones (Fig. 5c, d) indicate that growth was “disturbed” and the crystals did not maintain a euhedral habit throughout. Lobes preserved at the crystal margin define embayments, and are especially abundant in dykes in the lower GRV. Deeply embayed (“vermicular”) quartz has been reported in other shallow intrusions (e.g. Chang and Meinert, 2004). Embayments have been mostly interpreted as evidence of resorption resulting from temperature increase, depressurisation or compositional variations (magma mixing) (e.g. Bachmann et al., 2002; Nekvasil, 1991). However, the fact that some embayments reflect CL growth textures, rather than truncating them, indicates that resorption is not always responsible, as also suggested by other studies (e.g. Lowenstern, 1995; Müller et al., 2000).

Growth-related irregular or lobate textures may be due to a physical impediment such as a mineral of fluid phase stuck on the surface of the quartz crystal (Fig. 4e). However, in most cases shown in this study, no impediment is apparent (Fig. 5). During growth in the magma, crystals can depart from a flat geometry and develop bulges, depending on the degree of undercooling (oversaturation; MacLellan and Trembath, 1991). These “topographic” highs on the crystal surface will grow preferentially because of their higher degree of exposure to the elements necessary for crystallisation. Therefore, small irregularities in the surface, once created, may be enhanced by further crystallisation and evolve into wavy and lobate textures.

Although quartz embayments are not always due to resorption, there are other indicators of quartz resorption. Discordance between CL growth zones and grain margins (Fig. 4, 6c) indicate that quartz phenocrysts underwent multiple resorption episodes, implying that the magma shifted between silica-saturated and silica-undersaturated conditions.

6.2 Evidence for temperature increase

Assuming equilibrium crystallisation, trace element uptake of quartz is controlled by 1) magma composition, and 2) trace elements' quartz-melt distribution coefficients ($K_{Qtz/melt} = C_{Qtz}/C_{melt}$), in their turn influenced by the intensive parameters (P, T) and bulk melt composition. Therefore, progressive changes in trace element content of quartz may be expected as a consequence of normal compositional and thermal evolution, even in a magma crystallising as a closed system. Titanium content, in particular, is controlled by the equilibration temperature of quartz (Ti-in-quartz "TitaniQ" geothermometer; Wark and Watson, 2006) according to the equation:

$T(K) = -3765/[\log(X_{Ti}/aTi)-5.69]$,

where X_{Ti} is the content of Ti in quartz in ppm, and aTi is the activity of Ti in the coexisting melt. This relationship between Ti content and crystallisation temperature, and the correlation between CL intensity and Ti content (Fig. 7, 8) allow CL characteristics of each quartz grain to be used as an indicator of the crystallisation history of quartz.

Although the geothermometer was calibrated in Ti-saturated conditions (in the presence of rutile), it can also be applied to rutile-free magmas, provided that the activity of Ti is known. Most rhyolitic magmas are Ti-undersaturated, and aTi is typically in the interval 0.5-1 (e.g. Hayden and Watson, 2007; Wiebe et al., 2007). In the lower GRV, Ti oxide occurs 1) as an exsolution phase in Fe-Ti oxide; 2) in late-crystallised 'pockets' of minerals, together with zircon and apatite; and 3) as anhedral grains interstitial between groundmass crystals. Therefore, Ti oxide is not considered in equilibrium with the melt, implying aTi <1. Under these conditions, application of the geothermometer for aTi = 1 would give underestimated (minimum) temperatures.

Titanium activity can be estimated based on experimental work (Hayden and Watson, 2007) if an independent estimate of temperature is available. The zircon saturation model (Watson and Harrison, 1983) can be applied to felsic whole-rock samples and quartz-hosted melt inclusions (Agangi et al., under revision) to estimate magmatic temperatures (Table 2). We calculated Ti saturation concentration (ppm) using the model of Hayden and Watson (2007) at zircon saturation temperatures, and then obtained Ti activity by assuming Henrian behaviour, or aTi = Ti(measured)/Ti(saturation). This calculation yields average activity values of aTi ~0.60 (Fig. 9, Table 2).

Temperature estimates based on zircon saturation of the magma and on Ti content of quartz (Wark and Watson, 2006) overlap only partially (Fig. 9). Such mismatch of T estimates may be partially due to sampling bias (differences within and between units), and to the effect of pressure on Ti intake of quartz (Thomas et al., 2010). Further uncertainty can be added by the effect of F on the solubility of zircon (Keppler, 1993).

Despite the uncertainty in the application of the method, abrupt variations of Ti concentration in quartz crystals (step zones) are not consistent with a continuous compositional and thermal evolution of the magma. They reflect discrete events, and require sudden changes in the crystallisation conditions.

Although aTi has a profound influence on the estimates of crystallisation temperature, it only has a minor effect on the temperature difference between zones (ΔT, Fig. 10). Some quartz phenocrysts show bright CL rims around dark cores (e.g. Fig. 4a, e). These luminescent rims cross-cut internal growth zones and are associated with a rimwards increase in Ti content (reverse zoning). Under the assumption of constant pressure and aTi during crystallisation (the latter condition is achieved if TiO_2 was buffered by the crystallisation of Fe-Ti oxide), and assuming a value of aTi = 0.5, the measured Ti increase corresponds to a core-rim temperature increase of up to +70°C for the volcanic units (zones 1 to 3, Table 3). In the Moonamby Dyke Suite, core-mantle and mantle-rim maximum ΔT can be estimated in -150°C and +110°C, respectively. Temperature differences between quartz zones of >100°C have been reported previously (Smith et al., 2010; Wark et al., 2007).

Trace element diffusion profiles can be used to estimate residence time of crystals at high temperature (diffusion clock; Chakraborty, 2008). The largest Ti gradient measured between step zones is ~60 ppm over short distances of ≤10-20 µm (analyses 2-3, grain 70-14 line 1, Table 3). Assuming an initial step-like profile and considering Ti diffusivity in quartz (in the order of 10^{-22} m^2/s at 800°C; Cherniak et al., 2007), this gradient implies short residence time at high temperature (≤10^2-10^3 years) after crystallisation. Thus, the volcanic units and the dykes experienced rapid cooling by eruption and shallow emplacement shortly after quartz crystallisation, which prevented diffusion of Ti and allowed preservation of CL zones. Sharp CL zones and Ti gradients in volcanic units and dykes contrast with granite samples. We interpret the “smudged” CL zones of granite quartz as the result of slow cooling of these rocks.

6.3 Coexisting quartz populations with different crystallisation histories: magma chamber dynamics

One of the most prominent characteristics emerging from the study of quartz in the volcanic units of the lower GRV is the coexistence, in the same unit and even in the same sample, of crystal populations showing contrasting zoning patterns and trace element content (Fig. 4, 8). This observation suggests that quartz crystals formed under different conditions and were later mixed, and therefore implies a dynamic regime in the magma chamber (Fig. 11). In the volcanic units, CL-dark low-Ti (zone 1) and bright high-Ti (zone 2) quartz must have crystallised separately. Subsequently, quartz crystals underwent partial resorption (truncation of growth zones), either independently or after being juxtaposed. Finally, some of the resorbed crystals of quartz (1) and (2) underwent Si-(over)saturated conditions and crystallisation was resumed (zone 3).

The question can be asked whether these quartz populations were carried by melts with different origins and compositions that mixed in the lower GRV magma chamber. Resorption and disequilibrium textures have been widely used as evidence for magma mixing and crustal assimilation (e.g. Streck, 2008). Reverse zoning in quartz has been interpreted as evidence for an increase in either Ti and/or crystallisation temperature due to the injection of mafic magma into the magma chamber (Müller et al., 2005; Shane et al., 2008; Wark et al., 2007; Wark and

Watson, 2006; Wiebe et al., 2007).

Magma mixing and open-system processes have been shown to be common place in many felsic magmas on the basis of isotopic data showing crystal-melt disequilibrium (e.g. Charlier et al., 2007; Davidson et al., 2007; Martin et al., 2010), and injection of mafic magma at the base of felsic intrusions has been proven on the basis of field relationships (e.g. Turnbull et al., 2010; Wiebe et al., 2004). Basalt and basaltic andesite cropping out in the lower GRV (Blissett et al., 1993) and mafic igneous inclusions described in the upper GRV (Allen et al., 2003; Stewart, 1994), together with considerable variations of crystallisation temperatures between quartz zones, suggest the involvement of mafic magmas. On the other hand, mixing with a more mafic magma would cause an increase in Ca-femic components, and this would be expected to be reflected on the Fe content of quartz. This is not apparent from the microprobe analyses of quartz as Fe content does not correlate with Ti (Fig. 8). Therefore, although the data presented cannot give conclusive evidence of open-system processes in the GRV, mixing of mafic magma may have occurred in the rocks described here.

As an explanation for these features, we propose re-heating and convective stirring and overturning of the magma chamber (self-mixing; Couch et al., 2001). According to this model, hot mafic magma is intruded at the base of a silicic crystal-rich magma chamber; heat transfer forms a layer of hot and buoyant silicic magma that becomes unstable and rises in plumes. The rising plumes cause convection in the magma chamber, accounting for the coexistence of phenocrysts with different crystallisation histories. The temperature increase – possibly accompanied by magma contamination – explains resorption textures and the reverse zoning.

In contrast to the volcanic units, quartz zones and textures can be correlated among crystals within single dykes. This relationship implies common crystallisation conditions and shared crystallisation history, and indicates that quartz in dykes crystallised in a relatively stable, non-convecting portion of the magma, possibly roughly in situ (in the dykes).

One implication of this textural and compositional difference between extrusive and shallow intrusive units is that the dykes cannot be the “feeders” of the volcanic units. They may have fed units that are not any longer preserved in the area, or may represent injections of magma that never reached the surface.

Modern models of felsic igneous systems agree on the fact that magma chambers are mostly composed of largely solid crystal mush with interstitial melt (e.g. Bachmann and Bergantz, 2008), mostly incapable of bulk flow (Vigneresse et al., 1996). Large crustal intrusions are assembled incrementally, via successive injections of magma and do not exist as large volumes of molten rock at one time (Glazner et al., 2004; Lipman, 2007). Geophysical studies and drilling campaigns have failed to identify large pools of molten rock underneath volcanic systems (Detrick et al., 1990). Popular models of felsic magma chambers propose a zoned structure with largely solid margins, an intermediate crystal mush, and a melt-rich core-top (Hildreth, 2004; Hildreth and Wilson, 2007). Boundaries between these zones shift inwards and outwards, or "wax and wane", according to the thermal regime (Bachmann et al., 2002).

The mechanism proposed for the lower GRV is only apparently in conflict with existing models. In fact, mixing of crystal populations does not need the entire magma chamber to be largely molten at one time, and may occur locally in hotter volumes of magma located at the top or core of the chamber or in hot, rising plumes. A similar mechanism has been also applied to large felsic magma chambers to explain contrasting mineral textures (e.g. Fish Canyon Tuff; Bachmann et al., 2002).

6.4 Felsic enclaves: melting of a plutonic precursor

The felsic enclaves have similar mineralogical, textural, and compositional characteristics, in terms of both major and trace elements (Fig. 3), to the Hiltaba Suite granite and the GRV. Therefore, these enclaves are interpreted to be the product of partial re-melting of an early-crystallised portion of the GRV-HS magma, followed by a rapid cooling. Evidence of partial melting includes anhedral and lobate textures of quartz and K-feldspar, truncation of growth zones in quartz, and the presence of fine-grained groundmass (Fig. 6c). Rapid crystallisation of the partial melt is indicated by the granophyric rims (quenching coronas) on K-feldspar and the microcrystalline groundmass (Fig. 2c, d). Granophyric rims indicate eutectic growth of quartz and K-feldspar under conditions of moderate-high oversaturation (MacLellan and Trembath, 1991), most likely during eruption of the host lavas. Growth under conditions of high-oversaturation (quenching) may result from cooling at the surface and/or from increase of solidus temperature due to decompression. Similar textures in the Fish Canyon Tuff and the Alid volcanic field have been explained by rapid depressurisation and devolatilisation (Lipman et al., 1997; Lowenstern et al., 1997). Similar enclaves have been found in the upper GRV (Allen et al., 2003; Garner and McPhie, 1999), suggesting that the process of re-melting of granite continued during the second stage of the volcanic history of the province. Processes of re-melting of mostly or completely solid portions of the earlier granitoid magma and recycling of crystals have been inferred for other intermediate to silicic magmas (e.g. Bachmann et al., 2002, 2007; Charlier et al., 2005; Murphy et al., 2000).

7. Conclusions

Succession of quartz zones (step zones) with different compositions and textures ("crystal stratigraphy") records information on the crystallisation history. Primary (syn-crystallisation) CL textures in quartz are better preserved in rapidly cooled volcanic units and dykes of the lower GRV than in slowly cooled granite samples. Preservation of sharp Ti profiles suggests short residence time of quartz crystals at high temperature: eruption (or shallow emplacement of dykes) occurred shortly (10^2-10^3 years) after quartz crystallisation.

Different degrees of complexity can be observed in primary CL textures of quartz phenocryst. The simplest case occurs in the dykes, where zones can be correlated among quartz phenocrysts. The homogeneity of quartz populations in single dykes is interpreted as evidence that quartz crystals shared the same crystallisation history and probably crystallised largely after isolation of these small magma batches in intrusions. Embayments are common in quartz in the dykes and are mirrored by CL textures, suggesting that, in many cases, embayments had a primary (growth-related, rather than resorption-related) origin.

In the volcanic units, multiple quartz populations coexist in the same sample. Each of these populations records a complex history of crystallisation and resorption events. The volcanic units tapped a larger part of the magma characterised by a dynamic regime, which resulted in juxtaposition of different quartz populations, each with different crystallisation histories.

Geothermometric estimates based on Ti content of quartz zones suggest significant differences of quartz crystallisation temperatures (ΔT up to 70°C in volcanic units) between adjacent zones.

Alternating events of crystallisation and resorption (truncation of growth textures), reverse zoning (rimwards increase in Ti content) of quartz, and melting of already crystallised portions of the magma chamber (felsic enclaves) are consistent with non-monotonous thermal evolution of the GRV-HS magma and suggest the occurrence of different thermal “pulses”.

The described textural and microchemical features are best explained by re-heating and convective stirring of the magma chamber (self-mixing; Couch et al., 2001). Heat input represented both the “engine” for convection and the cause of re-melting of previously crystallised magma, and was possibly supplied by underplating of mafic magma. Open-system processes (injection of mafic magma and mixing with the felsic magma) may have played a role.

Acknowledgments

This research was funded by ARC-CODES grants to the authors. Field and logistical support was provided by the Primary Industries and Resources of South Australia (PIRSA). Dr. Karsten Gömann, Philip Robinson and Katie McGoldrick (University of Tasmania) are thanked for analytical assistance. The manuscript was significantly improved by the comments of two anonymous reviewers.

References

Agangi, A., Kamenetsky, V.S., McPhie, J., 2010. The role of fluorine in the concentration and transport of lithophile trace elements in felsic magmas: Insights from the Gawler Range Volcanics, South Australia. Chemical Geology 273, 314-325.

Allègre, C.J., Provost, A., Jaupart, C., 1981. Oscillatory zoning - a pathological case of crystal-growth. Nature 294, 223-228.

Allen, S.R., McPhie, J., 2002. The Eucarro Rhyolite, Gawler Range Volcanics, South Australia: a > 675 km^3, compositionally zoned lava of Mesoproterozoic age. Geological Society of America Bulletin 114, 1592-1609.

Allen, S.R., McPhie, J., Ferris, G., Simpson, C., 2008. Evolution and architecture of a large felsic igneous province in western Laurentia: The 1.6 Ga Gawler Range Volcanics, South Australia. Journal of Volcanology and Geothermal Research 172, 132-147.

Allen, S.R., Simpson, C.J., McPhie, J., Daly, S.J., 2003. Stratigraphy, distribution and geochemistry of widespread felsic volcanic units in the Mesoproterozoic Gawler Range Volcanics, South Australia. Australian Journal of Earth Sciences 50, 97-112.

Anderson, A.T., 1976. Magma mixing: petrological process and volcanological tool. Journal of Volcanology and Geothermal Research 1, 3-33.
Anderson, A.T., 1984. Probable relations between plagioclase zoning and magma dynamics, Fuego Volcano, Guatemala. American Mineralogist 69, 660-676.
Anderson, J.L., Morrison, J., 2005. Ilmenite, magnetite, and peraluminous Mesoproterozoic anorogenic granites of Laurentia and Baltica. Lithos 80, 45-60.
Bachmann, O., Bergantz, G.W., 2008. Rhyolites and their source mushes across tectonic settings. Journal of Petrology 49, 2277-2285.
Bachmann, O., Dungan, M.A., Lipman, P.W., 2002. The Fish Canyon magma body, San Juan volcanic field, Colorado: Rejuvenation and eruption of an upper-crustal batholith. Journal of Petrology 43, 1469-1503.
Bachmann, O., Miller, C.F., de Silva, S.L., 2007. The volcanic-plutonic connection as a stage for understanding crustal magmatism. Journal of Volcanology and Geothermal Research 167, 1-23.
Betts, P.G., Giles, D., 2006. The 1800-1100 Ma tectonic evolution of Australia. Precambrian Research 144, 92-125.
Blissett, A.H., 1975. Rock units in the Gawler Range Volcanics, South Australia. Geological Survey of South Australia, Quarterly Geological Notes 55, 2-14.
Blissett, A.H., 1977a. CHILDARA, Sheet SH/53-14, 1:250000 geological series. Geological Survey of South Australia, Adelaide.
Blissett, A.H., 1977b. GAIRDNER, Sheet SH/53-15, 1:250000 geological series. Geological Survey of South Australia, Adelaide.
Blissett, A.H., Creaser, R.A., Daly, S.J., Flint, R.B., Parker, A.J., 1993. Gawler Range Volcanics. In: J.F. Drexel, Preiss, W. V., Parker, A. J. (Editor), The geology of South Australia. Geological Survey of South Australia, Adelaide.
Boiron, M.C., Essarraj, S., Sellier, E., Cathelineau, M., Lespinasse, M., Poty, B., 1992. Identification of fluid inclusions in relation to their host microstructural domains in quartz by cathodoluminescence. Geochimica et Cosmochimica Acta 56, 175-185.
Bottinga, Y., Kudo, A., Weill, D., 1966. Some observations on oscillatory zoning and crystallization of magmatic plagioclase. American Mineralogist 51, 792-806.
Branch, C.D., 1978. Evolution of the middle Proterozoic Chandabooka Caldera, Gawler range acid volcano-plutonic province, South Australia. Journal of the Geological Society of Australia 25, 199-216.
Branney, M.J., Bonnichsen, B., Andrews, G. D. M., Ellis, B., Barry, T. L., McCurry, M., 2008. 'Snake River (SR)-type' volcanism at the Yellowstone hotspot track: distinctive products from unusual, high-temperature silicic super-eruptions. Bulletin of Volcanology 70, 293-314.
Bryan, S., 2007. Silicic Large Igneous Provinces. Episodes 30, 20-31.
Bryan, S.E., Ernst, R.E., 2008. Revised definition of large igneous provinces (LIPs). Earth-Science Reviews 86, 175-202.
Bryan, S.E., Ewart, A., Stephens, C.J., Parianos, J., Downes, P.J., 2000. The Whitsunday Volcanic Province, Central Queensland, Australia: lithological and stratigraphic investigations of a silicic-dominated large igneous province. Journal of Volcanology and Geothermal Research 99, 55-78.
Budd, A.R., Fraser, G.L., 2004. Geological relationships and $^{40}Ar/^{39}Ar$ age constraints on gold mineralisation at Tarcoola, central Gawler gold province, South Australia. Australian Journal of Earth Sciences 51, 685-699.
Cameron, M., Bagby, W.C., Cameron, K.L., 1980. Petrogenesis of voluminous mid-tertiary ignimbrites of the Sierra-Madre Occidental, Chihuahua, Mexico. Contributions to Mineralogy and Petrology 74, 271-284.
Chakraborty, S., 2008. Diffusion in solid silicates: a tool to track timescales of processes comes of age. Annual Review of Earth and Planetary Sciences 36, 153-190.
Chang, Z.S., Meinert, L.D., 2004. The magmatic-hydrothermal transition - evidence from quartz phenocryst textures and endoskarn abundance in Cu-Zn skarns at the Empire Mine, Idaho, USA. Chemical Geology 210, 149-171.
Charlier, B.L.A., Bachmann, O., Davidson, J.P., Dungan, M.A., Morgan, D.J., 2007. The upper crustal evolution of a large silicic magma body: Evidence from crystal-scale Rb-Sr isotopic

heterogeneities in the Fish Canyon magmatic system. Colorado. Journal of Petrology 48, 1875-1894.
Charlier, B.L.A., Wilson, C. J. N., Lowenstern, J.B., Blake, S., Van Calsteren, P.W., Davidson, J.P., 2005. Magma generation at a large, hyperactive silicic volcano (Taupo, New Zealand) revealed by U-Th and U-Pb systematics in zircons. Journal of Petrology 46, 3-32.
Cherniak, D.J., Watson, E.B., Wark, D.A., 2007. Ti diffusion in quartz. Chemical Geology 236, 65-74.
Couch, S., Sparks, R.S.J., Carroll, M.R., 2001. Mineral disequilibrium in lavas explained by convective self-mixing in open magma chambers. Nature 411, 1037-1039.
Creaser, R.A., 1995. Neodymium isotopic constraints for the origin of Mesoproterozoic felsic magmatism, Gawler-Craton, South Australia. Canadian Journal of Earth Sciences 32, 460-471.
Creaser, R.A., Cooper, J.A., 1993. U-Pb geochronology of Middle Proterozoic felsic magmatism surrounding the Olympic Dam Cu-U-Au-Ag and Moonta Cu-Au-Ag deposits, South Australia. Economic Geology and the Bulletin of the Society of Economic Geologists 88, 186-197.
Daly, S.J., Fanning, C.M., Fairclough, M.C., 1998. Tectonic evolution and exploration potential of the Gawler Craton, South Australia. AGSO Journal of Australian Geology and Geophysics 17, 145-168
Davidson, J.P., Morgan, D.J., Charlier, B.L.A., Harlou, R., Hora, J.M., 2007. Microsampling and isotopic analysis of igneous rocks: Implications for the study of magmatic systems. Annual Review of Earth and Planetary Sciences 35, 273-311.
Detrick, R.S., Mutter, J.C., Buhl, P., Kim, I.I., 1990. No evidence from multichannel reflection data for a crustal magma chamber in the MARK area on the Mid-Atlantic Ridge. Nature 347, 61-64.
D'Lemos, R.S., Kearsley, A.T., Pembroke, J.W., Watt, G.R., Wright, P., 1997. Complex quartz growth histories in granite revealed by scanning cathodoluminescence techniques. Geological Magazine 134, 549-552.
Fanning, C.M., Flint, R.B., Parker, A.J., Ludwig, K.R., Blissett, A.H., 1988. Refined Proterozoic evolution of the Gawler Craton, South-Australia, through U-Pb zircon geochronology. Precambrian Research 40-1, 363-386.
Ferrari, L., Lopez-Martinez, M., Rosas-Elguera, J., 2002. Ignimbrite flare-up and deformation in the southern Sierra Madre Occidental, western Mexico: Implications for the late subduction history of the Farallon plate. Tectonics 21, 17-1-17-24.
Ferris, G.M., 2001. The geology and geochemistry of granitoids in the Childara region, western Gawler craton, South Australia – implications for the Proterozoic tectonic history of the western Gawler craton and the development of lode-style gold mineralization at Tunkillia, University of Tasmania, Hobart, 175 pp.
Ferris, G.M., 2003. Volcanic textures within the Glyde Hill Volcanic Complex. Quarterly Earth Resources Journal of Primary Industries and Resources, South Australia 29, 36-41.
Flint, R.B., 1993. Hiltaba Suite. In: J.F. Drexel, Preiss, W.V., Parker, A.J. (Editor), The geology of South Australia. Geological Survey of South Australia, Adelaide, pp. 127-131.
Fraser, G.L., Skirrow, R.G., Schmidt-Mumm, A., Holm, O., 2007. Mesoproterozoic gold in the central Gawler craton, South Australia: Geology, alteration, fluids, and timing. Economic Geology 102, 1511-1539.
Frost, B. R., Barnes, C. G., Collins, W. J., Arculus, R. J., Ellis, D. J., Frost, C. D., 2001. A geochemical classification for granitic rocks. Journal of Petrology 42, 2033-2048.
Garner, A., McPhie, J., 1999. Partially melted lithic megablocks in the Yardea Dacite, Gawler Range Volcanics, Australia: implications for eruption and emplacement mechanisms. Bulletin of Volcanology 61, 396-410.
Giles, C.W., 1977. Rock units in the Gawler Range Volcanics, Lake Everard area, South Australia. Geological Survey of South Australia, Quarterly Geological Notes 51, 7-16.
Giles, C.W., 1988. Petrogenesis of the Proterozoic Gawler Range Volcanics, South-Australia. Precambrian Research 40-1, 407-427.
Ginibre, C., Wörner, G., Kronz, A., 2002. Minor- and trace-element zoning in plagioclase: implications for magma chamber processes at Parinacota volcano, northern Chile. Contributions to Mineralogy and Petrology 143, 300-315.

Glazner, A.F., Bartley, J.M., Coleman, D.S., Gray, W., Taylor, R.Z., 2004. Are plutons assembled over millions of years by amalgamation from small magma chambers? GSA Today 14, 4-11.

Götze, J., Plötze, M., Trautmann, T., 2005. Structure and luminescence characteristics of quartz from pegmatites. American Mineralogist 90, 13-21.

Hand, M., Reid, A., Jagodzinski, L., 2007. Tectonic framework and evolution of the Gawler craton, southern Australia. Economic Geology 102, 1377-1395.

Hayden, L.A., Watson, E.B., 2007. Rutile saturation in hydrous siliceous melts and its bearing on Ti-thermometry of quartz and zircon. Earth and Planetary Science Letters 258, 561-568.

Henry, C.D., Price, J. G., Rubin, J.N., Parker, D.F., Wolff, J.A., Self, S., Franklin, R., Barker, D.S., 1988. Widespread, lava-like silicic volcanic-rocks of Trans-Pecos Texas. Geology 16, 509-512.

Hildreth, W., 1981. Gradients in silicic magma chambers - implications for lithospheric magmatism. Journal of Geophysical Research 86, 153-192.

Hildreth, W., 2004. Volcanological perspectives on Long Valley, Mammoth Mountain, and Mono Craters: several contiguous but discrete systems. Journal of Volcanology and Geothermal Research 136, 169-198.

Hildreth, W., Wilson, C.J.N., 2007. Compositional zoning of the Bishop Tuff. Journal of Petrology 48, 951-999.

Keppler, H., 1993. Influence of fluorine on the enrichment of high-field strength trace-elements in granitic-rocks. Contributions to Mineralogy and Petrology 114, 479-488.

Lipman, P., Dungan, M., Bachmann, O., 1997. Comagmatic granophyric granite in the Fish Canyon Tuff, Colorado: Implications for magma-chamber processes during a large ash-flow eruption. Geology 25, 915-918.

Lipman, P.W., 2007. Incremental assembly and prolonged consolidation of Cordilleran magma chambers: Evidence from the Southern Rocky Mountain volcanic field. Geosphere 3, 42-70.

Lowenstern, J.B., 1995. Applications of silicate melt inclusions to the study of magmatic volatiles. In: J.F.H. Thompson (Editor), Magmas, fluids and ore deposits. Mineralogical Association of Canada Short Course, pp. 71-99.

Lowenstern, J.B., Clynne, M.A., Bullen, T.D., 1997. Comagmatic A-type granophyre and rhyolite from the Alid volcanic center, Eritrea, northeast Africa. Journal of Petrology 38, 1707-1721.

MacLellan, H.E., Trembath, L.T., 1991. The role of quartz crystallization in the development and preservation of igneous texture in granitic rocks; experimental evidence at 1 kbar. American Mineralogist 76, 1291-1305.

Martin, V.M., Davidson, J., Morgan, D., Jerram, D.A., 2010. Using the Sr isotope compositions of feldspars and glass to distinguish magma system components and dynamics. Geology 38, 539-542.

McPhie, J., DellaPasqua, F., Allen, S.R., Lackie, M.A., 2008. Extreme effusive eruptions: palaeoflow data on an extensive felsic lava in the Mesoproterozoic Gawler Range Volcanics. Journal of Volcanology and Geothermal Research 172, 148-161.

Müller A., van den Kerkhof A.M., Behr H.-J., Kronz A., Koch-Müller M., 2010 (for 2009). The evolution of late-Hercynian granites and rhyolites documented by quartz - a review. Earth and Environmental Science Transactions of the Royal Society of Edinburgh 100, 185-204.

Müller, A., Breiter, K., Seltmann, R., Pecskay, Z., 2005. Quartz and feldspar zoning in the eastern Erzgebirge volcano-plutonic complex (Germany, Czech Republic): evidence of multiple magma mixing. Lithos 80, 201-227.

Müller, A., Lennox, P., Trzebski, R., 2002. Cathodoluminescence and micro-structural evidence for crystallisation and deformation processes of granites in the Eastern Lachlan Fold Belt (SE Australia). Contributions to Mineralogy and Petrology 143, 510-524.

Müller, A., Rene, M., Behr, H.J., Kronz, A., 2003. Trace elements and cathodoluminescence of igneous quartz in topaz granites from the Hub Stock (Slavkovsky Les Mts., Czech Republic). Mineralogy and Petrology 79, 167-191.

Müller, A., Seltmann, R., Behr, H.J., 2000. Application of cathodoluminescence to magmatic quartz in a tin granite - case study from the Schellerhau Granite Complex, Eastern Erzgebirge, Germany. Mineralium Deposita 35, 169-189.

Murphy, M.D., Sparks, R.S.J., Barclay, J., Carroll, M.R., Brewer, T.S., 2000. Remobilization of andesite magma by intrusion of mafic magma at the Soufriere Hills Volcano, Montserrat, West Indies. Journal of Petrology 41, 21-42.

Nekvasil, H., 1991. Ascent of felsic magmas and formation of rapakivi. American Mineralogist 76, 1279-1290.

Pankhurst, R.J., Leat, P. T., Sruoga, P., Rapela, C. W., Marquez, M., Storey, B. C., Riley, T. R., 1998. The Chon Aike province of Patagonia and related rocks in West Antarctica: A silicic large igneous province. Journal of Volcanology and Geothermal Research 81, 113-136.

Pankhurst, R.J., Riley, T.R., Fanning, C.M., Kelley, S.P., 2000. Episodic silicic volcanism in Patagonia and the Antarctic Peninsula: chronology of magmatism associated with the break-up of Gondwana. Journal of Petrology 41, 605-625.

Peppard, B.T., Steele, I.M., Davis, A.M., Wallace, P.J., Anderson, A.T., 2001. Zoned quartz phenocrysts from the rhyolitic Bishop Tuff. American Mineralogist 86, 1034-1052.

Perny, B., Eberhardt, P., Ramseyer, K., Mullis, J., Pankrath, R., 1992. Microdistribution of Al, Li, and Na in alpha-quartz - Possible causes and correlation with short-lived cathodoluminescence. American Mineralogist 77, 534-544.

PIRSA (2006) Primary Industries and Resources of South Australia Geoscientific GIS Dataset (unpublished).

Rämö, O., Haapala, I., 1995. One hundred years of rapakivi granite. Mineralogy and Petrology 52, 129-185.

Riley, T.R., Leat, P.T., Pankhurst, R.J., Harris, C., 2001. Origins of large volume rhyolitic volcanism in the Antarctic Peninsula and Patagonia by crustal melting. Journal of Petrology 42, 1043-1065.

Sato, H., 1975. Diffusion coronas around quartz xenocrysts in andesite and basalt from Tertiary volcanic region in Northeastern Shikoku, Japan. Contributions to Mineralogy and Petrology 50, 49-64.

Shane, P., Smith, V.C., Nairn, I., 2008. Millennial timescale resolution of rhyolite magma recharge at Tarawera volcano: insights from quartz chemistry and melt inclusions. Contributions to Mineralogy and Petrology 156, 397-411.

Shore, M., Fowler, A.D., 1996. Oscillatory zoning in minerals: A common phenomenon. Canadian Mineralogist 34, 1111-1126.

Sibley, D.F., Vogel, T.A., Walker, B.M., Byerly, G., 1976. Origin of oscillatory zoning in plagioclase - Diffusion and growth controlled model. American Journal of Science 276, 275-284.

Skirrow, R.G., Bastrakov, E., Davidson, G.J., Raymond, O., Heithersay, P., 2002. Geological framework, distribution and controls of Fe-oxide Cu- Au deposits in the Gawler craton. Part II. Alteration and mineralization. In: T.M. Porter (Editor), Hydrothermal iron oxide copper-gold and related deposits. Porter GeoConsultancy, Adelaide, pp. 33-47.

Skirrow, R.G., Bastrakov, E.N., Baroncii, K., Fraser, G.L., Creaser, R.A., Fanning, C.M., Raymond, O.L., Davidson, G.J., 2007. Timing of iron oxide Cu-Au-(U) hydrothermal activity and Nd isotope constraints on metal sources in the Gawler craton, South Australia. Economic Geology 102, 1441-1470.

Smith, V., Shane, P., Nairn, I., 2010. Insights into silicic melt generation using plagioclase, quartz and melt inclusions from the caldera-forming Rotoiti eruption, Taupo volcanic zone, New Zealand. Contributions to Mineralogy and Petrology 160, 951-971.

Stewart, K.P., 1994. High temperature silicic volcanism and the role of mantle magmas in Proterozoic crustal growth: the Gawler Range Volcanic Province. University of Adelaide, Adelaide.

Streck, M.J., 2008. Mineral textures and zoning as evidence for open system processes. Reviews in Mineralogy and Geochemistry 69, 595-622.

Sun, S.S., McDonough, W.F., 1989. Chemical and isotopic systematics of oceanic basalts: implications for mantle composition and processes. In: A.D. Saunders, Norry, M. J. (Editor), Magmatism in the Ocean Basins. Geological Society of London, London, pp. 313-345.

Tepley, F.J., Davidson, J.P., Tilling, R.I., Arth, J.G., 2000. Magma mixing, recharge and eruption histories recorded in plagioclase phenocrysts from el Chichon Volcano, Mexico. Journal of Petrology 41, 1397-1411.

Thomas, J., Watson, B.E., Spear, F., Shemella, P., Nayak, S., Lanzirotti, A., 2010. TitaniQ under pressure: the effect of pressure and temperature on the solubility of Ti in quartz. Contributions to Mineralogy and Petrology 160, 743-759.
Turnbull, R. Weaver, S., Tulloch, A. Cole, J., Handler, M., Ireland, T., 2010. Field and geochemical constraints on mafic-felsic interactions, and processes in high-level arc magma chambers: an example from the Halfmoon Pluton, New Zealand. Journal of Petrology 51, 1477-1505.
Van den Kerkhof, A.M., Hein, U.F., 2001. Fluid inclusion petrography. Lithos 55, 27-47.
Vazquez, J., Reid, M., 2002. Time scales of magma storage and differentiation of voluminous high-silica rhyolites at Yellowstone caldera, Wyoming. Contributions to Mineralogy and Petrology 144, 274-285.
Vigneresse, J.L., Barbey, P., Cuney, M., 1996. Rheological transitions during partial melting and crystallization with application to felsic magma segregation and transfer. Journal of Petrology 37, 1579-1600.
Wallace, G., S., Bergantz, G.W., 2005. Reconciling heterogeneity in crystal zoning data: an application of shared characteristic diagrams at Chaos Crags, Lassen Volcanic Center, California. Contributions to Mineralogy and Petrology 149, 98-112.
Wark, D.A., Hildreth, W., Spear, F.S., Cherniak, D.J., Watson, E.B., 2007. Pre-eruption recharge of the Bishop magma system. Geology 35, 235-238.
Wark, D.A., Watson, E.B., 2006. TitaniQ: a titanium-in-quartz geothermometer. Contributions to Mineralogy and Petrology 152, 743-754.
Watson, E.B., Harrison, T.M., 1983. Zircon saturation revisited: temperature and composition effects in a variety of crustal magma types. Earth and Planetary Science Letters 64, 295-304.
Watt, G.R., Wright, P., Galloway, S., McLean, C., 1997. Cathodoluminescence and trace element zoning in quartz phenocrysts and xenocrysts. Geochimica et Cosmochimica Acta 61, 4337-4348.
Wiebe, R.A., 1968. Plagioclase stratigraphy - a record of magmatic conditions and events in a granite stock. American Journal of Science 266, 690-703.
Wiebe, R.A., Manon, M.R., Hawkins, D.P., McDonough, W.F., 2004. Late-stage mafic injection and thermal rejuvenation of the Vinalhaven Granite, Coastal Maine. Journal of Petrology 45, 2133-2153.
Wiebe, R.A., Wark, D.A., Hawkins, D.P., 2007. Insights from quartz cathodoluminescence zoning into crystallization of the Vinalhaven granite, coastal Maine. Contributions to Mineralogy and Petrology 154, 439-453.

Fig. 1. Interpreted geology of the Gawler Craton (after Daly et al., 1998; Betts and Giles, 2006, Hand et al., 2007). Inset shows the location of the Gawler Craton.

Fig. 2. Sample textures in the lower GRV. a Wheepool Rhyolite (sample GH23, GR 0517647-6488394). b Moonamby Dyke Suite (sample GH15, GR 0509965-6502023). c, d Felsic enclave (sample GH29, GR 0 524305-6495515). The enclave was included in the Whyeela Dacite (host not shown). d Granophyric rim around K-feldspar crystal in felsic enclave. All photomicrographs are in plane polarised transmitted light. GR: Grid reference GDA94. Abbreviations: Ab albite, Kfs K-feldspar, Qtz quartz.

Fig. 3. Whole-rock composition of the Gawler SLIP. Major oxides recalculated to 100% anhydrous and plotted as wt.%, trace elements as ppm. MALI: modified alkali-lime index, Na_2O+K_2O-CaO (Frost et al., 2001); ASI: alumina saturation index, Al/(Na+K+Ca), mol. Normalising values in primitive mantle-normalised plots after Sun and McDonough (1989). Small symbols in Harker diagrams: data from Giles (1988); Stewart (1994); Ferris (2001); PIRSA (2006). (*) From Agangi et al. (2010).

Fig. 4. Cathodoluminescence textures in the volcanic units of the lower GRV. a, b Quartz in the Wheepool Rhyolite (sample GH23). A thin bright overgrowth is locally present (arrowed). c, d Fractured crystals in the Waurea Pyroclastics (sample GH13, GR 0515415-6501451). e-g Quartz in the Lake Gairdner Rhyolite (sample GH51, GR 0524145-6542610). A sulfide grain constituted a mechanical growth impediment for the quartz crystal (e). For e-g growth textures are highlighted. Zones (*1*), (2) and (3) were not found together in the same grain. Growth textures (oscillatory zones) are parallel to subhedral grain margins in zone (*3*), except where fractured (top of f), but are truncated by round zone boundaries or grain margins in zones (*1*) and (*2*).

Fig. 5. Cathodoluminescence textures in dykes of the lower GRV. a Round mantle-rim boundary truncates the internal growth textures (arrowed). b The core is surrounded by a discontinuous mantle. c, d Disturbances of growth (wavy CL zones) coincide with melt inclusions or embayments. e Smudged CL; the crystal is crossed by CL-dark areas related to healed cracks (arrowed). a-c sample GH70 (GR 0491376-6490439); d sample GH15; e sample GH92 (GR 0486550-6489826).

Fig. 6. Cathodoluminescence textures in the Hiltaba Suite granite (a, b) and felsic enclaves in the lower GRV (c). a “Smudged” CL zones, Hiltaba Suite (sample GH37, GR 0517317-6546439). b Dark homogeneous areas with sharp borders are partly related to cracks (sample GH37). c Quartz grain from a felsic enclave in the Whyeela Dacite showing weak oscillatory zones (dashed lines) cross-cut by grain margin, dark lobate areas associated with fractures, and a thin discontinuous bright rim (sample GH29).

Fig. 7. Trace element concentrations in zones of quartz phenocrysts of the Moonamby Dyke Suite (a) and Lake Gairdner Rhyolite (b) compared with CL intensity. Titanium values show good correlation with CL emission. Trace element compositions are average analyses of parallel traverses and are expressed as ppm, CL as panchromatic 0-255 grey scale.

Fig. 8. Trace element composition and CL relative intensity of quartz in the volcanic units and the Moonamby Dyke Suite. Elements as ppm, CL as 0-255 grey scale. Standard deviation for Al less than symbol size. LGR Lake Gairdner Rhyolite, WP Waurea Pyroclastics, *(1)-(3)* quartz zones (see text).

Fig. 9. Quartz crystallisation temperature (TitaniQ geothermometer; Wark and Watson, 2006) compared with rutile solubility model (Hayden and Watson, 2007). Quartz crystallisation temperature modelled Ti activity aTi = 0.6 in the melt. Whole-rock and melt inclusion data from Table 3.

Fig. 10. Influence of Ti activity (aTi) on Ti-in-quartz geothermometry (TitaniQ geothermometer, Wark and Watson, 2006). Ti activity has significant influence on estimates of crystallisation temperature (a), but only minor influence on ΔT between crystal zones (b). Moonamby Dyke Suite, sample GH70, quartz grain 70-10.

Fig. 11. Conceptual model for the crystallisation of quartz in the lower GRV magma chamber.

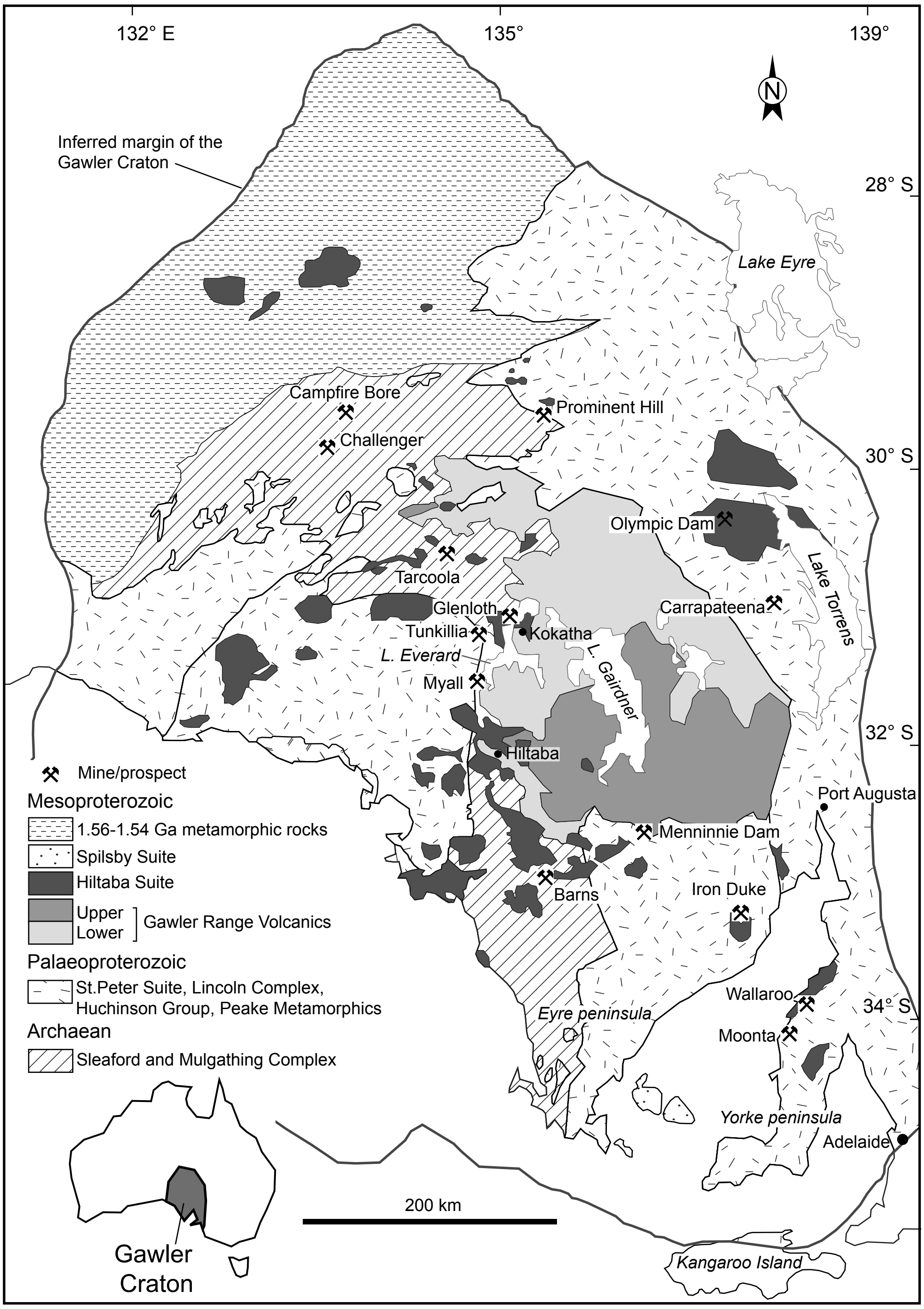

132° E
135°
139°
N
Inferred margin of the Gawler Craton
28° S
Lake Eyre
Campfire Bore
Prominent Hill
Challenger
30° S
Olympic Dam
Tarcoola
Carrapateena
Lake Torrens
Glenloth
Tunkillia
Kokatha
L. Everard
L. Gairdner
Myall
32° S
Hiltaba
Mine/prospect
Mesoproterozoic
1.56-1.54 Ga metamorphic rocks
Spilsby Suite
Hiltaba Suite
Upper
Lower
Gawler Range Volcanics
Palaeoproterozoic
St.Peter Suite, Lincoln Complex, Huchinson Group, Peake Metamorphics
Archaean
Sleaford and Mulgathing Complex
Port Augusta
Menninnie Dam
Barns
Iron Duke
Wallaroo
34° S
Eyre peninsula
Moonta
Yorke peninsula
Adelaide
200 km
Gawler Craton
Kangaroo Island

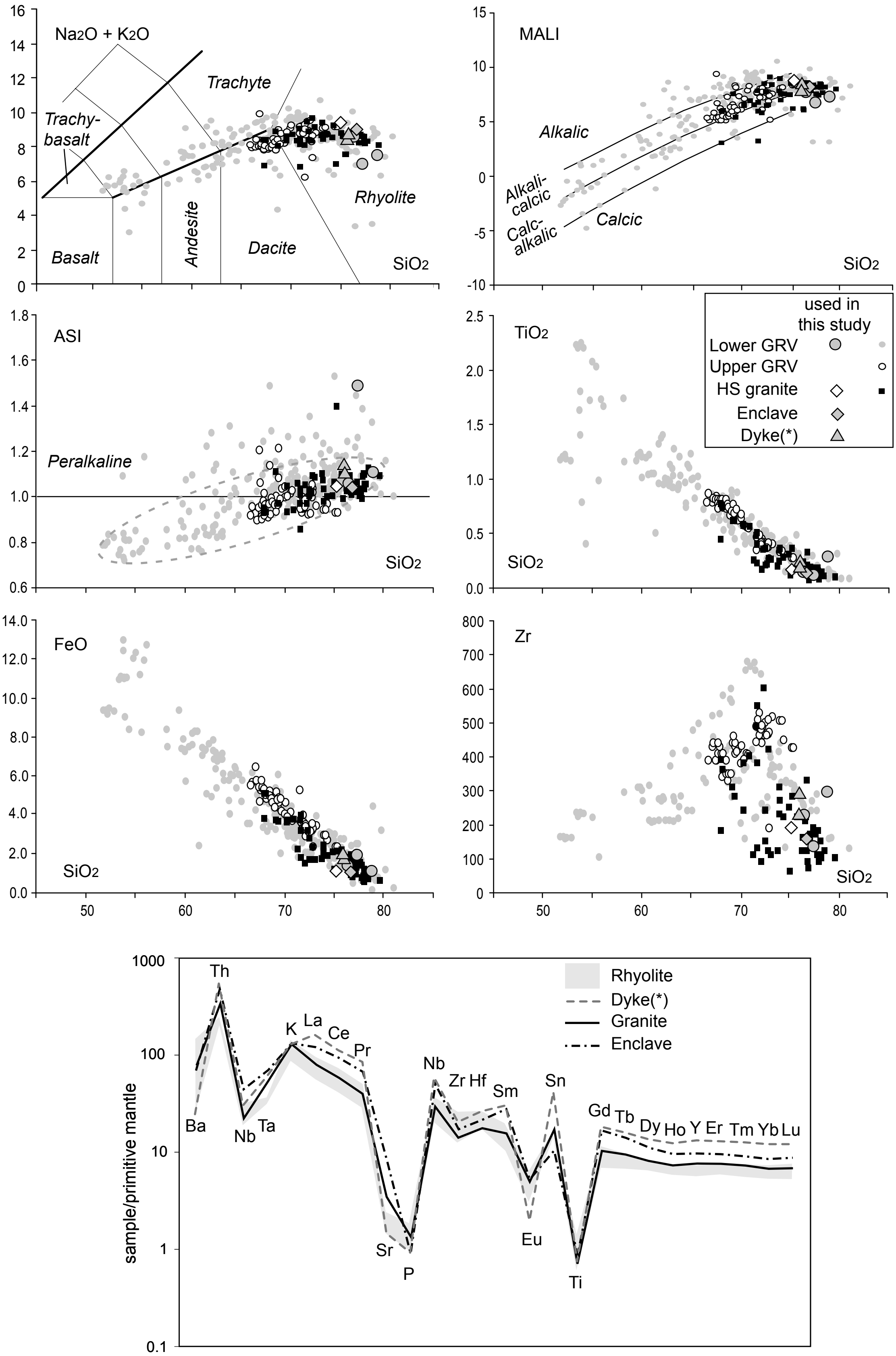

Na2O + K2O
Trachy-basalt
Trachyte
Basalt
Andesite
Dacite
Rhyolite
SiO2
MALI
Alkalic
Alkali-calcic
Calc-alkalic
Calcic
SiO2
ASI
Peralkaline
SiO2
TiO2
SiO2
used in this study
Lower GRV
Upper GRV
HS granite
Enclave
Dyke(*)
FeO
SiO2
Zr
SiO2
Rhyolite
Dyke(*)
Granite
Enclave
sample/primitive mantle
Th
Ba
Nb
Ta
K
La
Ce
Pr
Sr
P
Nb
Zr
Hf
Sm
Eu
Sn
Ti
Gd
Tb
Dy
Ho
Y
Er
Tm
Yb
Lu

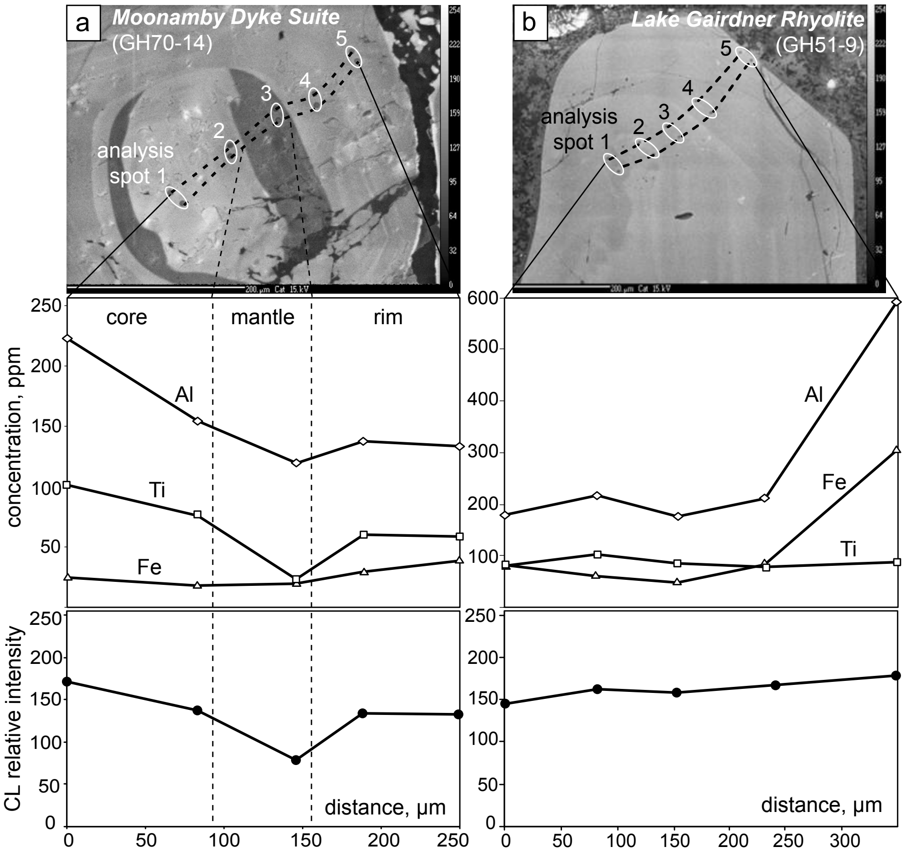
a
Moonamby Dyke Suite
(GH70-14)
analysis
spot 1
2
3
4
5
b
Lake Gairdner Rhyolite
(GH51-9)
core
mantle
rim
Al
Ti
Fe
concentration, ppm
CL relative intensity
distance, µm

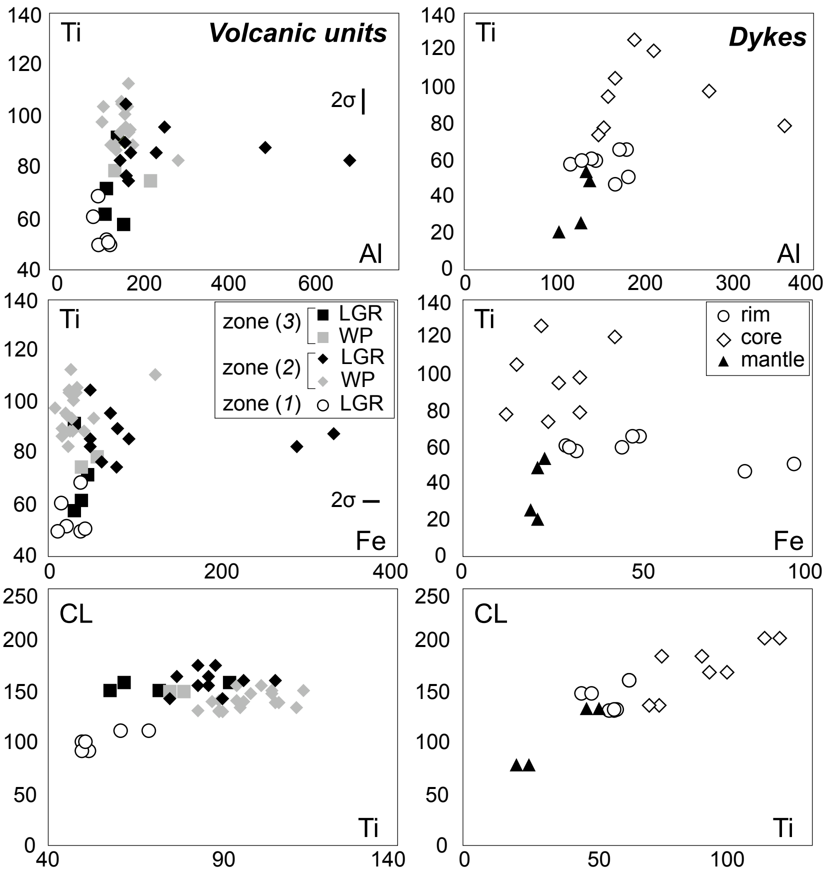

Volcanic units
Dykes
Ti
Al
Fe
CL
2σ
zone (3)
LGR
WP
zone (2)
LGR
WP
zone (1)
LGR
rim
core
mantle

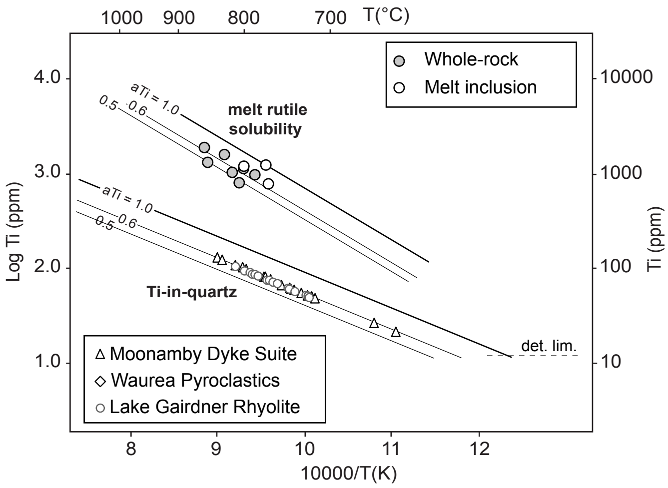

T(°C)
1000
900
800
700
Whole-rock
Melt inclusion
aTi = 1.0
0.6
0.5
melt rutile solubility
Ti-in-quartz
det. lim.
Moonamby Dyke Suite
Waurea Pyroclastics
Lake Gairdner Rhyolite
Log Ti (ppm)
4.0
3.0
2.0
1.0
Ti (ppm)
10000
1000
100
10
8
9
10
11
12
10000/T(K)

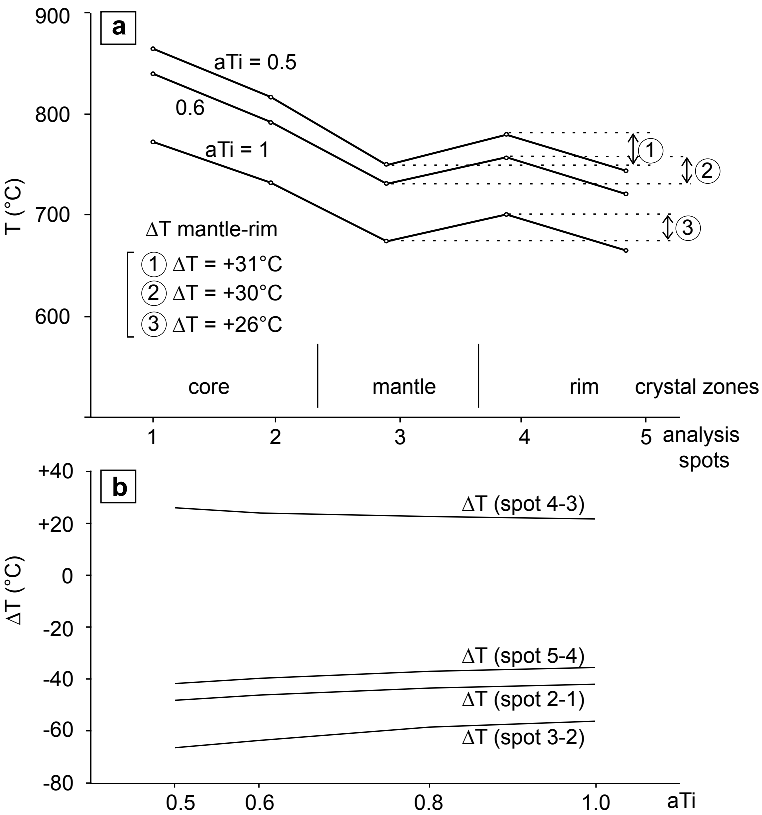

a
900
800
700
600
T (°C)
aTi = 0.5
0.6
aTi = 1
ΔT mantle-rim
1 ΔT = +31°C
2 ΔT = +30°C
3 ΔT = +26°C
core
mantle
rim
crystal zones
1
2
3
4
5
analysis spots
b
+40
+20
0
-20
-40
-60
-80
ΔT (°C)
ΔT (spot 4-3)
ΔT (spot 5-4)
ΔT (spot 2-1)
ΔT (spot 3-2)
0.5
0.6
0.8
1.0
aTi

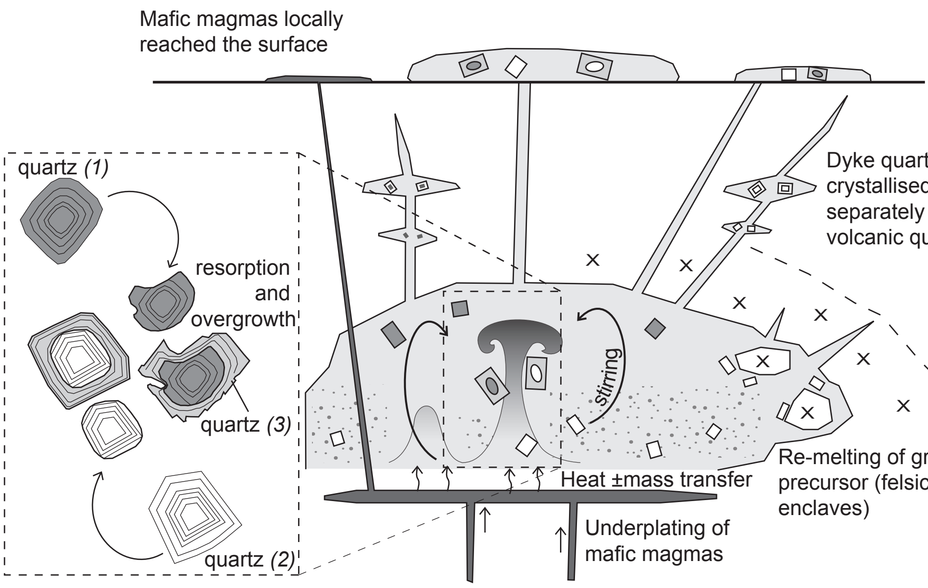

Mafic magmas locally
reached the surface
quartz (1)
resorption
and
overgrowth
quartz (3)
quartz (2)
Dyke quartz
crystallised
separately from
volcanic quartz
stirring
Re-melting of granite
precursor (felsic
enclaves)
Heat ±mass transfer
Underplating of
mafic magmas

- Quartz trace elements and cathodoluminescence as a record of magmatic conditions
- Ti-in-quartz geothermometry indicates large T variations between quartz zones
- Resorption textures and reverse zoning indicate pulsating temperature conditions

Table 1: Textural and compositional characteristics of selected quartz-bearing units in the lower GRV

Unit	Wheepool Rhyolite	Lake Gairdner Rhyolite	Waurea Pyroclastics	Yantea Rhyolite-dacite	Whyeela Dacite	Moonamby Dyke Suite	Hiltaba Suite
Locality	Lake Everard	Kokatha	Lake Everard	Lake Everard	Lake Everard	Lake Everard	Kokatha
Emplacement mode	lava	ignimbrite	ignimbrite	lava	lava	shallow intrusion	intrusion
Texture	porphyritic	massive-eutaxitic	massive-eutaxitic	porphyritic	porphyritic	porphyritic	equigranular-seriate
Max grain size	≤5 mm	≤2 mm	≤2 mm	≤5 mm	≤2 mm	≤3 cm	≤10 mm
Phenocrysts/ crystals	Ab, Kfs, Qtz	Qtz, Kfs, Ab	Kfs, Qtz, Ab	Ab, ±Qtz	Ab, ±Qtz	Qtz, Ab, Kfs	Qtz, Kfs, Ab, Bt
Groundmass/matrix	Qtz, Kfs, Ab	Kfs, Qtz, Fe ox	Qtz, Kfs	Ab, Kfs, Qtz	Ab, Kfs, Qtz	Qtz, Ab, Kfs	
Accessory minerals	Ap, Zrn, Fe-Ti ox, ±REE-F-Cb, ±Mnz, ±Ti ox	Ttn, Zrn, Fe-Ti ox	Fe ox, Ti ox, Fl, Zrn	Fe ox, Ap, Zrn, Ti ox, ±REE-F-Cb	Fe-Ti ox, Ap, Fl, Zrn	Fe ox, Ti ox, Fl, Ap, Zrn, REE-F-Cb	Fe ox, Fl, Zrn, Ap
Groundmass/matrix texture	microcrystalline (< 50 µm)	vitriclastic (≤ 500 µm)	vitriclastic (≤ 300 µm)	microcrystalline-micropoikilitic (≤ 50 µm)	microcrystalline-granophyric (≤ 50 µm)	microcrystalline (≤ 100 µm), poikilitic Qtz	–
Phenocryst abundance/ crystal proportion	10%	20%	<20%	10%	<10%	20-30%	–
Quartz abundance	≤1% (phenocryst)	10% (crystal)	5-10% (crystal)	<1% (uneven distribution)	<1% (uneven distribution)	5-10% (phenocryst)	20-30%
Felsic enclaves	-	-	-	X	X	-	-

Abbreviations: Ab albite, Am amphibole, Ap apatite, Bt biotite, Cb carbonate, Cpx clinopyroxene, Fl fluorite, Kfs K-feldspar, Mag magnetite, Mnz monazite, ox oxide, Qtz quartz, Ttn titanite, Zrn zircon.

Table 2. Whole-rock and average melt inclusion compositions

Sample		GH06	GH13	GH51	GH15*	GH70*	GH37
Unit	detection limits	Wheepool Rhyolite	Waurea Pyroclastics	Lake Gairdner Rhyolite	Moonamby Dyke Suite	Moonamby Dyke Suite	Hiltaba Suite
SiO2 (wt.%)		78.16	74.85	75.67	75.60	75.16	76.25
TiO2		0.29	0.12	0.19	0.16	0.23	0.15
Al2O3		11.23	11.93	12.10	11.88	12.19	12.12
Fe2O3		1.24	2.10	2.20	1.56	2.03	1.21
MnO		0.03	0.03	0.11	0.06	0.01	0.02
MgO		0.53	0.83	0.24	0.44	0.34	0.23
CaO		0.11	0.17	0.46	0.69	0.14	0.60
Na2O		3.47	1.04	1.87	2.54	2.93	2.91
K2O		4.00	5.68	6.61	5.95	5.63	5.83
P2O5		0.04	0.02	0.02	0.02	0.05	0.03
BaO		0.12	0.03	0.19	0.07	0.19	0.10
loss(inc S-)		0.97	2.81	0.44	1.37	1.00	0.50
Cl							
F							
S		<0.01	<0.01	<0.01	<0.01	0.01	<0.01
Total		100.19	99.62	100.10	100.34	99.90	99.95
Li (ppm)	0.016	9.99	14.46	5.74	12.99	7.56	10.69
Be	0.008	2.00	2.41	2.30	4.35	3.64	3.27
B							
Sc	0.038	4.63	3.31	6.10	3.43	4.05	2.69
Ti	1.203	1805.33	766.69	1259.09	985.65	1509.00	930.95
V (XRF)	1.5	14.10	5.70	4.40	1.50	8.60	2.00
Cr (XRF)	1	2	2	4	2	3	1
Mn	0.410	230.66	203.42	930.83	457.51	100.51	171.85
Ni (XRF)	1	4	3	4	5	5	4
Cu (XRF)	1	1	3	6	2	2	4
Zn (XRF)	1	29	43	49	37	28	23
Ga	0.025	10.63	13.56	17.25	15.29	14.91	16.71
As	5	<5	10.36	<5	<5	<5	<5
Rb	0.044	117.36	211.03	226.47	312.05	271.64	266.91
Sr (XRF)	1	51	31	50	31	78	71
Y	0.005	33.68	29.24	26.22	60.37	44.09	35.00
Zr	0.035	299.49	138.58	292.85	231.02	232.69	161.66
Nb (XRF)	1	19	22	14	22	20	16
Mo	0.023	0.14	0.54	0.66	1.11	0.46	0.82
Ag	0.010	0.03	0.05	0.10	0.04	0.05	0.08
Cd	0.024	<0.23	<0.23	<0.23	<0.23	<0.23	<0.23
Sn	0.011	2.87	2.50	2.63	7.21	4.19	2.94
Sb	0.053	0.21	0.54	<0.06	0.44	0.11	0.21
Te	0.091	<0.37	<0.37	<0.37	<0.37	<0.37	<0.37
Cs	0.004	1.27	3.33	4.23	3.47	2.38	3.67
Ba (XRF)	4	584	199	1067	175	983	568
La	2	39.80	40.41	66.98	111.97	79.90	58.57
Ce	0.012	130.97	71.51	131.76	202.50	164.71	98.74
Pr	0.002	10.99	8.05	14.59	23.62	17.63	11.87
Nd	0.009	43.26	27.67	51.47	79.99	58.78	41.65
Sm	0.007	8.85	4.76	8.21	13.70	9.89	7.12
Eu	0.002	1.00	0.52	1.14	0.33	0.87	0.85
Gd	0.006	7.04	4.20	6.33	10.96	8.09	6.37
Tb	0.001	1.08	0.76	0.93	1.73	1.33	1.03

Dy	0.004	6.12	4.85	5.13	10.14	7.80	6.08
Ho	0.001	1.23	1.02	0.98	2.05	1.56	1.21
Er	0.003	3.79	3.28	2.90	6.21	4.90	3.65
Tm	0.003	0.57	0.53	0.42	0.94	0.76	0.55
Yb	0.003	3.66	3.58	2.63	5.97	5.05	3.46
Lu	0.003	0.57	0.56	0.40	0.91	0.78	0.53
Hf	0.004	8.40	5.59	7.87	8.21	7.59	5.54
Ta	0.002	1.51	1.28	1.29	2.50	2.35	2.26
Tl	0.010	0.64	1.01	1.12	1.43	1.25	1.40
Pb (XRF)	1.5	10	11	42	7	8	37
Bi	0.010	0.16	0.01	0.12	0.06	0.09	0.67
Th	0.002	17.82	21.78	19.35	47.07	45.68	27.09
U	0.002	2.69	1.31	3.84	9.17	2.47	1.75
Zrn sat T(°C)**		858	809	852	820	829	787
aTi		0.63	0.45	0.45	0.48	0.68	0.66

Major elements by XRF, trace elements by ICP-MS, except where XRF is indicated, melt inclusion

* from Agangi et al. (2010)

** Zircon saturation temperature (Watson and Harrison, 1983)

	Melt inclusion average	Melt inclusion average	Melt inclusion average
GH32			
Felsic enclave	Moonamby Dyke Suite	Waurea Pyroclastics	Wheepool Rhyolite
74.66	76.41	77.46	73.25
0.17	0.19	0.16	0.17
12.95	12.07	12.66	14.22
1.25	1.28	0.55	0.92
0.05	<dl	<dl	<dl
0.31	0.02	<dl	0.11
0.54	0.58	0.29	0.47
3.22	4.11	3.33	3.88
6.08	4.86	5.25	6.15
0.02	<dl	<dl	<dl
0.10	<dl	<dl	<dl
0.82			
	0.11	0.07	0.07
	0.31	0.09	0.65
<0.01	<dl	<dl	<dl
100.17	99.94	99.87	99.89
5.17	13.71	28.14	15.49
3.72	6.03	<dl	4.41
	26.55	<dl	21.24
4.19			
1112.93	1163.37	740.53	1241.44
4.10			
1			
421.01			
4			
2	55	1154	234
18	43	53	55
17.00	16.71	14.95	16.14
9.12			
259.29	367.17	303.91	311.11
169	12	0	15
45.30	52.33	18.12	34.25
193.87	209.03	119.80	143.02
32	24	27	25
16.38			
1.52			
<0.23			
1.75	9.58	4.26	5.22
0.10			
<0.37			
3.40	9.63	8.02	10.10
456	62	2	115
83.29	86.87	17.56	46.74
163.53	191.05	36.04	104.08
18.46	17.88	3.03	10.39
67.47	65.89	9.25	36.11
12.37	10.31	1.86	6.78
0.87	0.39	<dl	0.60
10.05	10.16	1.29	5.84
1.53	1.43	0.38	0.98

8.26	9.10	2.19	5.71
1.57	1.86	0.47	1.12
4.50	5.70	2.15	3.56
0.66	0.89	0.34	0.59
4.09	5.51	2.75	3.84
0.62	0.85	0.29	0.59
6.77	7.17	5.14	5.40
2.84	1.76	1.62	1.64
1.31			
21	46	41	41
0.01			
40.86	43.04	19.08	26.69
0.93	10.32	5.33	6.76
802	801	771	774
0.66	0.69	0.68	1.03

ı data (EPMA and LA-ICP-MS) from Agangi et al. (under revision)

Table 3. Quartz trace element analyses (EPMA, ppm) and crystallisation temperatures

Quartz grain	analysis # (centre-rim)	Unit	Al	Fe	Ti	CL relative intensity	Quartz zone	T, °C (aTi=1)
Qtz 13-13 line1	1	WP	3347	123	111	136	2	760
	2	WP	167	25	105	141	2	753
	3	WP	125	25	104	150	2	752
	4	WP	174	30	101	158	2	748
	5	WP	232	39	75	152	3	714
Qtz 13-13 line2	1	WP	186	23	95	136	2	741
	2	WP	166	34	106	141	2	754
	3	WP	122	9	98	150	2	745
	4	WP	183	28	94	158	2	740
	5	WP	151	57	79	152	3	719
Qtz 13-6 line1	1	WP	173	17	90	132	2	734
	2	WP	180	33	104	153	2	752
	3	WP	154	17	87	142	2	730
	4	WP	142	26	89	133	2	733
	5	WP	152	42	89	143	2	733
Qtz 13-6 line2	1	WP	192	29	89	132	2	733
	2	WP	182	27	113	153	2	762
	3	WP	176	21	96	142	2	742
	4	WP	295	24	83	133	2	725
	5	WP	164	53	94	143	2	740
Qtz 51-9 line1	1	LGR	174	80	90	145	2	734
	2	LGR	264	72	96	163	2	742
	3	LGR	163	49	83	158	2	725
	4	LGR	245	93	86	167	2	729
	5	LGR	685	284	83	178	2	725
Qtz 51-9 line2	1	LGR	182	79	75	145	2	714
	2	LGR	176	49	105	163	2	753
	3	LGR	187	49	86	158	2	729
	4	LGR	177	62	77	167	2	716
	5	LGR	493	326	88	178	2	732
Qtz 51-4 line1	1	LGR	102	16	61	113	1	691
	2	LGR	132	22	52	93	1	674
	3	LGR	114	38	50	102	1	670
	4	LGR	157	31	92	161	3	737
	5	LGR	171	31	58	153	3	685
Qtz 51-4 line2	1	LGR	113	38	69	113	1	704
	2	LGR	140	12	50	93	1	670
	3	LGR	136	43	51	102	1	672
	4	LGR	129	39	62	161	3	693
	5	LGR	132	46	72	153	3	709
Qtz 70-14 line1	1	MDS	278	33	98	171	core	745
	2	MDS	158	12	78	138	core	718
	3	MDS	107	21	21	79	mantle	588
	4	MDS	133	30	60	134	rim	689
	5	MDS	120	32	58	133	rim	685
Qtz 70-14 line2	1	MDS	171	15	105	171	core	753
	2	MDS	152	24	74	138	core	712
	3	MDS	132	19	26	79	mantle	607
	4	MDS	144	29	61	134	rim	691
	5	MDS	149	45	60	133	rim	689
Qtz 70-10 line1	1	MDS	193	22	126	205	core	776
	2	MDS	364	33	79	187	core	719

	3	MDS	138	23	54	135	mantle	678
	4	MDS	176	48	66	163	rim	699
	5	MDS	171	80	47	150	rim	664
Qtz 70-10 line2	1	MDS	215	43	120	205	core	769
	2	MDS	163	27	95	187	core	741
	3	MDS	142	21	49	135	mantle	668
	4	MDS	184	50	66	163	rim	699
	5	MDS	186	94	51	150	rim	672
Avg								716
Max								776
Min								588

WP: Waurea Pyroclastics, LGR: Lake Gairdner Rhyolite, MDS: Moonamby Dyke Suite

T, °C (aTi=0.6)	T, °C (aTi=0.5)
827	853
819	845
818	843
814	839
774	798
805	830
820	846
809	835
804	829
781	805
798	823
818	843
794	818
797	821
797	821
797	821
829	855
807	832
787	812
804	829
798	823
807	832
787	812
792	816
787	812
774	798
819	845
792	816
778	802
795	820
749	771
730	752
725	747
801	826
743	765
764	787
725	747
728	749
751	773
769	793
809	835
779	803
634	652
747	769
743	765
819	845
773	796
655	674
749	771
747	769
845	872
781	805

734	756
758	781
718	739
838	864
805	830
723	744
758	781
728	749
778	801
845	872
634	652